Microstructure evolution and phase analysis of Sm60Ni40 alloy

G. Vijayaragavan, D. Prabhu, M.B. Ponnuchamy, K.R.S. Preethi Meher, Ravi Gautam, Mainak Saha, R. Gopalan, K.G. Pradeep

Journal of Magnetism and Magnetic Materials

Microstructure evolution and phase analysis of Sm60Ni40 alloy

--Manuscript Draft--

Manuscript Number:	MAGMA-D-22-01746
Article Type:	Full Length Article
Section/Category:	
Keywords:	Sm-Ni alloy; Annealing; Microstructure; Magnetic property and Crystal structure
Corresponding Author:	Prabhu Delhi Babu Chennai, India
First Author:	Prabhu Delhi Babu, Ph. D
Order of Authors:	Prabhu Delhi Babu, Ph. D
	G. Vijayaragavan
	M. B. Ponnuchamy
	K. R. S. Preethi Meher
	Ravi Gautam
	Mainak Saha
	R. Gopalan
	K. G. Pradeep
Abstract:	The paper investigates the microstructure evolution and phase analysis of the Sm 60 Ni 40 alloy. The arc melted sample retained the high temperature stable (> 600 °C) Sm 7 Ni 3 and Sm 3 Ni 2 phases along with the congruently melting SmNi phase. Annealing the as-cast sample at 630 o C for 100 hours stabilized the high temperature stable (600 °C - 630 °C) Sm 3 Ni 2 phase. Rietveld refinement was performed to resolve the crystal structure of Sm 3 Ni 2 phase and it was observed that Sm 3 Ni 2 phase stabilizes in monoclinic crystal structure (space group: C2/m) with a lattice parameter of a=13.49 Å, b=3.75 Å, c=9.68 Å and β=106.6°. The Curie temperature of the Sm 3 Ni 2 phase was determined to be ~110 K. The high squareness ratio of 82% along with high coercivity of 3 T indicates that the Sm 3 Ni 2 phase possess spontaneous uniaxial magnetic anisotropy.
Suggested Reviewers:	Ivan Skorvanek, Ph. D skorvi@saske.sk
	Nicoleta Lupu nicole@phys-iasi.ro
	Oksana Golovnia golovnya@imp.uran.ru

15th August 2022

From
Dr. D. Prabhu
International Advanced Research Centre for
Powder Metallurgy and New Materials (ARCI)
Chennai – 600113
Tamil Nadu
India

To
Prof. H. S. Kim
Editor
Intermetallics

Dear Professor
I am submitting herewith a manuscript titled "**Microstructure evolution and phase analysis of $Sm_{60}Ni_{40}$ alloy"** by G.Vijayaragavan, D. Prabhu, M. B. Ponnuchamy, K. R. S. Preethi Meher, Ravi Gautam, Mainak Saha, R. Gopalan, K. G. Pradeep, to be considered for publication in Intermetallics.

Sm based binary alloy systems with low melting eutectics are studied with interest as they are considered potential bonding materials for consolidation of Sm-Fe-N magnets at low temperatures. Sm-Ni is one such system with one of the eutectic reactions at 630 ºC. In this report, we present the experimental results on the microstructure and phase evolution of the Sm60Ni40 alloy both in as cast and annealed (630 °C for 100 hr) states in comparison with the thermodynamically predicted phase formation sequence at various temperatures. Interestingly, we were able to stabilize significant (80% area fraction) proportion of the high temperature stable Sm_3Ni_2 phase at room temperature. Though the crystal structure of this phase is reported in Open quantum material database OQMD to be rhombohedral based on DFT calculations with certain assumptions, in the present work our experimental observation is providing a **new information i.e. the structure of Sm_3Ni_2 being Monoclinic** in contrast from the one reported in OQMD. We have also resolved the crystal structural of Sm_3Ni_2 phase using XRD Rietveld analysis an information which was not available in literature prior to this work. Further, we have also reported the magnetic properties of this phase in this paper.

We believe the information provided in this paper is novel and would be most suitable to the journal exclusively dedicated to "intermetallics", and we hope you will find it worthy of publication in your valued journal.

Thank you
Yours sincerely
On behalf of the team of authors,

(D PRABHU)

Highlights of the paper

- The paper reports the structural and magnetic properties of a high temperature stable Sm_3Ni_2 phase, not reported experimentally earlier in literature to the best of our knowledge.
- The structure is determined to be monoclinic (space group C2/m) with a Curie temperature of 110 K.

Microstructure evolution and phase analysis of $Sm_{60}Ni_{40}$ alloy

G. Vijayaragavan[1,2], D. Prabhu[1,*], M. B. Ponnuchamy[2], K. R. S. Preethi Meher[3], Ravi Gautam[1], Mainak Saha[2], R. Gopalan[1], K. G. Pradeep[2,*]

[1]*Centre for Automotive Energy Materials (CAEM), International Advanced Research Centre for Powder Metallurgy and New materials (ARCI), Chennai, 600 113, India.*

[2]*Correlative Microscopy laboratory, Department of Metallurgical and Materials Engineering, Indian Institute of Technology Madras, Chennai, 600 036, India.*

[3]*Central University of Tamil Nadu, Neelakudi, Thiruvarur, Tamil Nadu 610 005, India*

[*]*Corresponding author:*

Email address: dprabhu@arci.res.in; kgprad@iitm.ac.in

Telephone no: +91 44 266632811; +91 44 22574764

Abstract:

The paper investigates the microstructure evolution and phase analysis of the $Sm_{60}Ni_{40}$ alloy. The arc melted sample retained the high temperature stable (> 600 °C) Sm_7Ni_3 and Sm_3Ni_2 phases along with the congruently melting SmNi phase. Annealing the as-cast sample at 630 °C for 100 hours stabilized the high temperature stable (600 °C - 630 °C) Sm_3Ni_2 phase. Rietveld refinement was performed to resolve the crystal structure of Sm_3Ni_2 phase and it was observed that Sm_3Ni_2 phase stabilizes in monoclinic crystal structure (space group: C2/m) with a lattice parameter of a=13.49 Å, b=3.75 Å, c=9.68 Å and β=106.6°. The Curie temperature of the Sm_3Ni_2 phase was determined to be ~110 K. The high squareness ratio of 82% along with high coercivity of 3 T indicates that the Sm_3Ni_2 phase possess spontaneous uniaxial magnetic anisotropy.

Keywords: Sm-Ni alloy, Annealing, Microstructure, Magnetic property and Crystal structure

1. Introduction

Recently, Sm-based low melting eutectics are being explored in literature as a potential metal binder for consolidation of Sm-Fe-N due to its good wettability and strong reducing ability [1]. In particular, Sm-Cu and Sm-Ni based alloy systems with eutectic melting points below the decomposition temperature of $Sm_2Fe_{17}N_3$ are considered prospective materials.

Sm-Ni binary system consisting of multiple eutectic compositions could be explored for its suitability as an ideal binder alloy. Recently, a few reports emerged investigating the phase formation in Sm-Ni system. Pan et al. [2] studied the Sm-Ni system across the entire composition range and developed the phase diagram using differential thermal analysis and X-ray diffraction techniques. SmNi and $SmNi_5$, Sm_3Ni were identified to be congruently melting phases while, $SmNi_2$, $SmNi_3$, Sm_2Ni_7, Sm_5Ni_{19} and Sm_2Ni_{17} phases form by peritectic reaction.

The binary Sm-Ni phase diagram has further been evaluated by Xuping et al. [3] and the observations were consistent with the reported literature. Independently, G. Borzone et al. [4] reported the formation of two new metastable phases Sm_3Ni_2 and Sm_7Ni_3 by peritectic reaction which decompose at temperature below 600 and 619 ℃ respectively. The crystal structure of the Sm_7Ni_3 phase was reported based on the indexing of diffraction pattern to hp20-Fe_3Th_7 structure type. To the best of our knowledge, no experimental data has been reported for the crystal structure of Sm_3Ni_2 apart from the one available in the open quantum data base which is theoretically predicted structure using density function theory calculations [5][6]. However, intermetallic phases with composition R_3Ni_2 form via peritectic reaction as reported in the literature for R = Tb, Dy, Ho, Er, Y and Gd. The crystallographic information is also available for Tb_3Ni_2, Dy_3Ni_2, Ho_3Ni_2, Er_3Ni_2 and Gd_3Ni_2 compounds. Monoclinic structure for Tb_3Ni_2 and Dy_3Ni_2 [Dy_3Ni_2 type, mS20, C2/m] [7], hexagonal for Er_3Ni_2 [Er_3Ni_2 type, hR45, R-3] [8] and tetragonal structure for Y_3Ni_2 [Y_3Ni_2 type , tP80 , $P4_12_12$] [9] exist. The Ho_3Ni_2 exist at low temperature [Dy_3Ni_2 type, mS20, C2/m] [7] as well as at high temperatures [Er_3Ni_2 type, hR45, R-3] [8]. Recently, monoclinic structure was reported for Gd_3Ni_2 [Dy_3Ni_2 type, mS20, C2/m] with lattice parameters [a = 1.3418, b = 0.372, c = 0.9640 nm and β = 106.2 °] [10]. In this study, we have investigated the Sm-Ni system close to the eutectic reaction (E3) having substantially lower reaction temperature (623 °C) as indicated in Fig. 1a. i.e. a fixed Ni content of 40 at. % towards understanding the microstructure evolution, phase stability and their magnetic properties.

2. Experimental details

The $Sm_{60}Ni_{40}$ (at. %) composition was melted using vacuum arc melting technique under inert Argon atmosphere. Elemental Samarium (Sm) and Nickel (Ni) with purity higher than 99.9% was used for preparing the alloy ingots. To compensate for the losses during melting, 1 wt.% excess Sm was added. In order to understand the phase formation as a function of temperature,

Sm-Ni phase diagram was generated using CALPHAD (Calculation of Phase Diagram) approach with the thermodynamic data available elsewhere [NIMS CPDDB (https://mits.nims.go.jp)] [11], [12]. The annealing temperature of 630 °C for 100 hours just above the corresponding eutectic reaction temperature (i.e. 623 °C for the composition under study) was determined from the phase diagram in order to obtain a homogeneous microstructure. The arc melted bulk alloy ingot was wrapped in a tantalum foil and sealed in a quartz tube filled partially with argon for heat treatment.

Phase analysis and crystal structure investigation were carried out by X-Ray diffraction (XRD) using Cu-k_α radiation (Panalytical, X'pert pro, Netherlands). The XRD patterns were obtained from fine powder samples by crushing the as-cast and annealed ingots. Phase identification of the as-cast sample was performed utilizing crystallographic data from the Inorganic Materials Database (Atom Work) of NIMS, Japan (https://mits.nims.go.jp) [13]. The XRD pattern of annealed samples were subjected to Rietveld refinement using Fullprof software for discerning the different phases. Crystal structure information of R_3Ni_2 stoichiometry phases with other rare earths such as Tb, Dy, Ho, Er, Y, Gd is available in literature [10]. The XRD patterns were fit using pseudo-Voigt profile with axial divergence asymmetry. Microstructure imaging and composition analysis was performed using FEG-Scanning electron microscope (SEM) (Zeiss, Merlin Compact, Germany) attached with an energy dispersive X-ray spectrometer (EDS) (EDAX, Octane plus, USA). Three-dimensional elemental distribution analysis at near atomic-scale was performed using a local electrode atom probe tomography (LEAP) (Cameca, 5000XR, USA). Site-specific atom probe tomography (APT) tips was prepared using a dual-beam Focused ion beam (FIB) (Thermofisher scientific, Helios G4 UX) following the lift out procedure described elsewhere [14],[15]. APT measurement was carried out in the laser pulsing mode with laser pulse frequency of 250 kHz and 30 pJ pulse energy while the tips were maintained at 60 K. Data reconstruction and analysis was performed using IVAS 3.8.10

software provided by Cameca Inc. The magnetic properties were measured using Physical property measurement system (PPMS) with vibrating sample magnetometer attachment (Quantum Design, Dynacool, USA). The Magnetisation (M) vs Applied Field (H) measurements were carried out from 300 K down to 20 K by applying a magnetic field between +9 T to –9 T. Thermomagnetic (Zero field cooled and Field cooled) measurements were carried out in the temperature range of 20 K to 300 K with an applied field of 0.05 T and 5 T.

3. Results and Discussion

Fig. 1a shows the generated equilibrium phase diagram of Sm-Ni. It can be noticed that 3 different eutectic reactions namely, E1 (1275 °C), E2 (821 °C) and E3 (623 °C) are possible, and it can be observed that the reaction temperature decreases with increasing Sm content. Table 1 summarizes all the possible reactions and the associated phases that are products of the various reactions [12]. The enlarged portion (in fig. 1b) shows the phase field around E3 where the composition under study lies. The schematic of microstructure evolution as a function of temperature is shown for the desired composition of $Sm_{60}Ni_{40}$ in fig. 1b. Accordingly, the ideal microstructure at room temperate should consist of SmNi and Sm_3Ni with phase fraction of 60 and 40 vol.% respectively. Fig. 2(a) shows the backscattered electron (BSE) image of the as cast sample. Three different phases corresponding to varying contrast (dark, white, and grey phase) are identified. To estimate the composition of the individual phases, EDS line scan was performed along the red dotted line shown in fig. 2(a) cutting across the three phases. The concentration profile obtained from EDS is shown in fig 2(b) and the three phases could be identified as SmNi (dark), Sm_7Ni_3 (white) and Sm_3Ni_2 (grey). The intensity distribution of Sm and Ni in the elemental map (fig. 2 (c & d)) is in agreement with the concentration profile. The as-cast microstructure consisting of high temperature stable Sm_7Ni_3 and Sm_3Ni_2 phases retained along with SmNi suggests non-equilibrium solidification of the molten liquid due to the water-cooling of the copper mold used in the arc melting furnace. According to fig. 1b,

SmNi should be the first solid phase emerging out of the $Sm_{60}Ni_{40}$ liquid phase at 850 °C as indicated in the schematic. Upon further solidification, a peritectic reaction between the remaining liquid and SmNi solid phase is expected at 630 °C. The observation of Sm_3Ni_2 being spatially separated from the SmNi phase suggests the suppression of peritectic reaction [P1 in table.1]. The remaining liquid therefore should have undergone eutectic solidification at 623 °C resulting in the formation of 17 Vol.% Sm_3Ni_2 and 43 Vol.% Sm_7Ni_3 phases. However, the thermodynamically predicted phase fraction of Sm_3Ni_2 and Sm_7Ni_3 phases at 623 °C are 12 Vol.% and 46 Vol. % respectively, indicating no further phase change.

Fig 3. shows the XRD powder diffraction pattern of the as-cast sample. Most of the peaks correspond to the SmNi and Sm_7Ni_3 phases. Few unknown peaks were observed which did not correspond to either of the phases. it is plausible that Sm_3Ni_2 phase (detected in SEM analysis) could contribute to diffraction resulting in the observation of additional peaks. However, it should be noted that, peak position was not in agreement with crystal structure predicted in OQMD for Sm_3Ni_2 [5][6].

Therefore, to obtain equilibrium microstructure, the sample was annealed at 630 ℃ for 100 h based on fig. 1b followed by furnace cooling. Fig. 4 shows the Rietveld refined XRD pattern for the annealed sample which indicates the presence of Sm_3Ni_2 and SmNi phases. The microstructure of the annealed sample is shown in fig. 5a which contains three different regions of varying contrast. The grey contrast region appears to be the major phase while the dark and white regions are present as minor fractions. SEM-EDS line scan was carried out along the red dotted line shown in fig. 5a cutting across all three contrasting regions to obtain their local chemical composition. Fig. 5b shows the concentration profile and based on the contents of Sm and Ni present, the three phases were identified to be Sm_3Ni_2 (~80 % area fraction, grey phase), SmNi (~10 % area fraction, dark phase) and Sm_3Ni (~10% area fraction, white phase). The elemental maps of Sm and Ni corresponding to the BSE image in fig. 5a confirm the

presence of three phases. The sporadic distribution of equilibrium SmNi and Sm_3Ni phases along with their spatially separated nature suggest that the precipitation of these two phases are due to the partial decomposition of the Sm_3Ni_2 phase below 600 ℃. Further, close observation of the Sm_3Ni precipitate (in fig. 5c) revealed an intragranular phase contrast which are distinct, indicative of the coexistence of multiple phases within, possibly in their metastable states. SEM-EDS line scan performed along the dotted line in fig. 5c does not show any significant variation in chemical composition across the metastable region which was also confirmed by the elemental mapping in fig. 5d. To further ascertain their phase constituents, site-specific APT measurement was performed along the multiphase contrast (metastable) region. Fig. 6a shows the elemental distribution map of Ni which appears to be inhomogeneous. 1D concentration profile along a 10 nm diameter cylindrical region of interest indicates local composition variations corresponding to Sm, SmNi, Sm_3Ni and Sm-Ni-O. To further visualize the distribution of Oxygen rich regions, and to determine their local chemical composition, an 8 at.% isoconcentration surface was used to delineate the atom map of O as shown in inset of Fig. 6b. The proximity histogram corresponding to one of the O rich regions (marked in rectangle) is constituted with 24.9 ± 0.89 at.% O, 15.8 ± 0.75 at.% Ni and 59.1 ± 1.01 at.% Sm. Significant amount of O seems to have been incorporated in the sample post-annealing even though annealing was performed under controlled Ar atmosphere. Based on the APT determined local chemical composition, it can be inferred that the Oxygen rich regions could be metastable and may not be related to any stable oxide phases. However, the Sm_3Ni_2 is resolved to be monoclinic with space group C2/m. The refined lattice parameter values are a = 13.487 Å, b = 3.754 Å, and c = 9.682 Å & $\beta = 106.6°$ different from the crystal structure and parameters reported in the OQMD for this structure [5][6]. However, it could be noted that the reported data is similar to isostructural Gd_3Ni_2 reported by et al [10].

Having stabilized significant fraction (80% area fraction) of high-temperature stable Sm_3Ni_2 phase in the annealed condition, detailed magnetic property evaluation has been performed. The temperature dependent magnetization measured with an applied field of 500 Oe for the as-cast alloy is shown in fig. 7a which shows two magnetic transitions. The first transition identified as T_{C1} at 45 K correspond to the curie temperature of SmNi compound which was found to be in good agreement with the value reported in literature [16],[17]. The second Curie transition identified as T_{C2} at 110 K should be that of either Sm_7Ni_3 or Sm_3Ni_2, but it could not be ascertained as the magnetic properties of these high temperature phases are not yet reported. Fig.7b shows the hysteresis loop measured for the as-cast alloy at 20 K (below T_{C1}), 100 K (below T_{C2}) and 120 K (above T_{C2}). The hysteresis loop at 20 K exhibited a two-phase behaviour suggesting that two ferromagnetic phases are magnetically decoupled. At 100 K (above the T_C of SmNi phase), a well-defined hysteresis loop can be observed with a coercivity of 1 kOe corresponding to either of Sm_7Ni_3 or Sm_3Ni_2 phases. At 120 K, the hysteresis vanishes and a linear change in magnetization typical of a paramagnetic behaviour observed since it is well above the curie temperature of all the ferromagnetic phases present in the as-cast alloy.

Figure 8a. shows the temperature dependent magnetization curve measured for the annealed sample which contains ~80% (area fraction) of Sm_3Ni_2 phase. The Curie transition at 45 K (T_{C1} i.e. of SmNi) was observed but only as a small slope change due to the low volume fraction of the SmNi phase present in the annealed sample. Whereas the T_{C2} remained similar to the as-cast sample at 110 K. The inset shows the derivative of the M vs T to clearly identify the two Curie transition temperatures. Based on the SEM microstructure obtained area fraction of phases and taking into account the thermomagnetic behaviour of the as-cast and annealed samples, the transition at 110 K should correspond to the Curie temperature of Sm_3Ni_2 phase. The Sm_7Ni_3 and Sm_3Ni phases present in the as-cast and annealed samples respectively may

be diamagnetic or have a Curie temperature below 5 K. The hysteresis loop of the annealed sample shown in fig. 8b is similar to the as-cast sample for the 120 K and 100 K. The dominant Sm_3Ni_2 phase present in the annealed sample exhibits a very high coercivity ~ 3 T at 20 K. The high coercivity and squareness (82%) of the hysteresis loop clearly suggests that the Sm_3Ni_2 is a hard magnetic phase with high uniaxial anisotropy. The high magnetocrystalline anisotropy of the Sm_3Ni_2 phase could be due to the Sm ion having a positive Stevens coefficient ($\alpha_J = 4 \times 10^{-2}$) [18] with a prolate shell [19]. The large separation distance between the zero-field cooled and field cooled thermomagnetic measurements carried out at an applied field of 5 T for the annealed sample shown in fig. 8b as inset further confirms the strong anisotropy of the Sm_3Ni_2 phase [20]. Recently, it was reported that Sm based alloys could act as binders for the consolidation of Sm-Fe-N powders. The magnetic properties of the binder alloy which will be present in the intergranular/interparticle regions is crucial and is considered favourable if they are paramagnetic as they can decouple the ferromagnetic interactions. The paramagnetic nature of Sm_3Ni_2 phase at room temperature highlights the possibility of further exploration as a potential binder material towards consolidation of Sm-Fe-N based bulk magnets.

4. Summary

The microstructure evolution, phase formation and magnetic properties of $Sm_{60}Ni_{40}$ alloy both in as cast and annealed (630 °C for 100h) conditions were investigated. The major observations are summarized below,

1. Significant fractions (~80% area fraction) of high temperature stable Sm_3Ni_2 can be stabilized at room temperature by annealing the as-cast material slightly above the E3 temperature.
2. The crystal structure of Sm_3Ni_2 phase has been determined using XRD Rietveld analysis to be monoclinic.
3. At room temperature Sm_3Ni_2 phase is paramagnetic which can exhibit high uniaxial magnetocrystalline anisotropy below 110K.
4. The very high coercivity of ~ 3 T observed at 20 K combined with 82% squareness ratio confirms the hard magnetic nature of Sm_3Ni_2 phase.

Based on the above observations, it can be concluded that appropriate heat treatment protocols could be devised to synthesize phase pure Sm_3Ni_2 alloy which offers the potential of utilizing them as binder material for the synthesis of high-performance Sm-Fe-N based bulk magnets.

Table.1. shows reaction in enlarged portion of the Sm-Ni phase diagram [12]

Reaction	Type	Temperature (℃)	ID
$L \rightarrow \alpha$ - Sm + Sm_2Ni_{17}	Eutectic	1275	E1
$L \rightarrow SmNi + SmNi_2$	Eutectic	821	E2
$L \rightarrow Sm_3Ni_2 + Sm_7Ni_3$	Eutectic	623	E3
$L + SmNi \rightarrow Sm_3Ni_2$	Peritectic	630	P1
$L + Sm_3Ni \rightarrow Sm_7Ni_3$	Peritectic	652	P2

Acknowledgements

This work was funded by Department of Science and Technology (DST), Govt. of India under BRICS project (DST/IMRCD/BRICS/PilotCall1/Nanomag-SmCoFe/2017(G)). The authors would like to acknowledge Dr. Tata Narasinga Rao, Director, ARCI for his constant support. Authors like to thank Mr. Goutam for experimental support in materials processing, Dr. S. Kavita and Mr. Debendra Nath Kar for PPMS measurements and Mr. Chandrasekhar for preparing the APT samples. Authors are grateful to Dr. K. Guruvidyathri, Assistant Professor, School of Engineering Sciences and Technology, University of Hyderabad for the fruitful technical discussion in this work and Thermocalc software learning. Authors acknowledge the support of National Facility for Atom Probe Tomography for performing APT measurements. GV, MBP, MS and KGP acknowledge the funding support from Ministry of Education through the Institute of Eminence (IoE) initiative for establishing the Center of Excellence in Correlative Microscopy. KGP is also grateful for the funding support from Science and Engineering Research Board (SERB) under the project No. ECR/2018/002938.

References:

[1] K. Otogawa, K. Takagi, T. Asahi, Consolidation of $Sm_2Fe_{17}N_3$ magnets with Sm-based eutectic alloy binder, J. Alloys Compd. 746 (2018) 19–26. https://doi.org/10.1016/j.jallcom.2018.02.266.

[2] Y. Pan, Z. Jian-xuan, A phase diagram of the alloys of the samarium-nickel binary system, J. Acta Phys. Synica. 32 (1983) 92–95. https://doi.org/10.7498/aps.32.92.

[3] X. Su, W. Zhang, Z. Du, A thermodynamic assessment of the Ni-Sm system, J. Alloys Compd. 278 (1998) 182–184. https://doi.org/10.1016/S0925-8388(98)00560-X.

[4] G. Borzone, Y. Yuan, S. Delsante, N. Parodi, The Sm-Ni system: new phases in the Sm-rich region, Monatsh Chem. 143 (2012) 1299–1307. https://doi.org/10.1007/s00706-012-0794-5.

[5] S. Kirklin, J.E. Saal, B. Meredig, A. Thompson, J.W. Doak, M. Aykol, S. Rühl, C. Wolverton, The Open Quantum Materials Database (OQMD): Assessing the accuracy of DFT formation energies, Npj Comput. Mater. 1 (2015). https://doi.org/10.1038/npjcompumats.2015.10.

[6] C. Saal, J. E., Kirklin, S., Aykol, M., Meredig, B., and Wolverton, Materials Design and Discovery with High-Throughput Density Functional Theory: The Open Quantum Materials Database (OQMD), JOM. 65 (2013) 1501–1509. https://doi.org/10.1007/s11837-013-0755-4.

[7] J.M. Moreau, D. Paccard, E. Parthé, The monoclinic, CrB-related, crystal structure of Tb_3Ni_2, Dy_3Ni_2 and Ho_3Ni_2, Acta Crystallogr. B30 (1974) 2583–2586. https://doi.org/10.1107/s0567740874007631.

[8] J.M.Moreau, D.Paccard, D.Gignoux, The crystal structure of Er_3Ni_2, Acta Crystallogr. B30 (1974) 2122–2126. https://doi.org/10.1016/j.ssc.2010.01.002.

[9] J. Le Roy, J. M. Moreau, D. Paccard, E. Parthé, Y_3Ni_2 : A New Tetragonal Phase with Ni-Centred Trigonal Prisms, Acta Crystallogr. B33 (1977) 3406–3409. https://doi.org/DOI:10.1107/S0567740877011091.

[10] A. Provino, V. Smetana, D. Paudyal, K.A. Gschneidner Jr, A.-V. Mudring, V.K. Pecharsky, P. Manfrinetti, M. Putti, Gd_3Ni_2 and $Gd_3Co_xNi_{2-x}$: magnetism and unexpected Co/Ni crystallographic ordering, J. Mater. Chem. C. 4 (2016) 6078–6089. https://doi.org/10.1039/C6TC01035K.

[11] National Institute for Materials Science Computational phase diagram database, https://mits.nims.go.jp (accessed January 20, 2022).

[12] Z. Rahou, K. Mahdouk, Thermodynamic reassessment of the Sm-Ni binary system, J. Alloys Compd. 664 (2016) 469–475. https://doi.org/10.1016/j.jallcom.2015.12.215.

[13] National Institute for Materials Science Inorganic materials database AtomWork, http://crystdb.nims.go.jp (accessed January 20, 2022).

[14] H. Zhang, K.G. Pradeep, S. Mandal, D. Ponge, H. Springer, D. Raabe, Dynamic strain-induced transformation: An atomic scale investigation, Scr. Mater. 109 (2015) 23–27. https://doi.org/10.1016/j.scriptamat.2015.07.010.

[15] I. Basu, K.G. Pradeep, C. Mießen, L.A. Barrales-Mora, T. Al-Samman, The role of atomic scale segregation in designing highly ductile magnesium alloys, Acta Mater. 116 (2016) 77–94. https://doi.org/10.1016/j.actamat.2016.06.024.

[16] S.C. Abrahams, J.L. Bernstein, R.C. Sherwood, J.H. Wernick, H.J. Williams, The crystal

structure and magnetic properties of the rare-earth nickel (RNi) compunds, J. Phys. Chem. Solids,. 25 (1964) 1069–1080. https://doi.org/10.1016/0022-3697(64)90129-5.

[17] Y. Isikawa, K. Mori, K. Ueno, K. Sato, K. Maezawa, Magnetic crystalline anisotropy of SmNi single crystal, J. Magn. Magn. Mater. 52 (1985) 434–436. https://doi.org/10.1016/0304-8853(85)90325-7.

[18] Robert C. O'Handley, Modern magnetic materials, Wiley (1999).

[19] R. Skomski, D.J. Sellmyer, Anisotropy of rare-earth magnets, J. Rare Earths. 27 (2009) 675–679. https://doi.org/https://doi.org/10.1016/S1002-0721(08)60314-2.

[20] P.A. Joy, P.S.A. Kumar, S.K. Date, The relationship between field-cooled and zero-field-cooled susceptibilities of some ordered magnetic systems, J. Phys. Condens. Matter. 10 (1998) 11049–11054. https://doi.org/10.1088/0953-8984/10/48/024.

Figure captions

Fig. 1 a) Sm-Ni binary phase diagram b) Enlarged region around the $Sm_{60}Ni_{40}$ composition with the inset schematic presenting the evolution of phases and microstructure as a function of temperature.

Fig. 2 (a) SEM-BSE microstructure of the as cast $Sm_{60}Ni_{40}$ alloy; (b) 1D concentration profile obtained along the dotted line (red color) in (a); EDX elemental map of (c) Sm and (d) Ni.

Fig. 3 X-ray diffraction pattern of the as cast sample obtained in powder form.

Fig. 4 X-ray diffraction pattern (red) of the annealed sample (630 °C for 100h) in powder form overlayed with the Rietveld refined pattern (in black).

Fig. 5 (a) SEM-BSE microstructure of the annealed sample (630 °C for 100h); (b) 1D concentration profile obtained along the dotted line (red color) in (a) along with the corresponding elemental maps of Sm and Ni. (c) Magnified SEM-BSE image of the Sm_3Ni precipitate showing the metastable intragranular region; (d) 1D concentration profile obtained along the dotted line (red color) in (c) along with the corresponding elemental maps of Sm and Ni.

Fig. 6 a) Elemental distribution map of Ni along with the 1D concentration profile obtained along a 10 nm diameter cylindrical region of interest with 0.5 nm bin width; (b) Oxygen rich regions in the elemental map (inset) delineated with 8 at.% isoconcentration surface and the representative proximity histogram obtained from the rectangular (red color) region with 0.1 nm bin width. Inset SEM-BSE micrograph also shows the region of interest (ROI) from where site-specific APT tips were prepared for composition analysis.

Fig. 7 a) Thermomagnetic curve of the as-cast sample showing two curie transitions at T_{C1} and T_{C2}; b) Hysteresis loop measured at various temperatures showing the magnetic property of the as-cast alloy.

Fig. 8 a) Thermomagnetic curve of the annealed sample showing two curie transitions at T_{C1} and T_{C2} and inset shows the derivative of the curve highlighting the two indicated transitions. b) Hysteresis loop measured at various temperatures showing the high coercivity of the Sm_3Ni_2 phase and inset shows the difference (vertical double headed arrow) between FC and ZFC measured for the annealed sample with an applied field of 5 T exhibiting the anisotropy of the Sm_3Ni_2 phase.

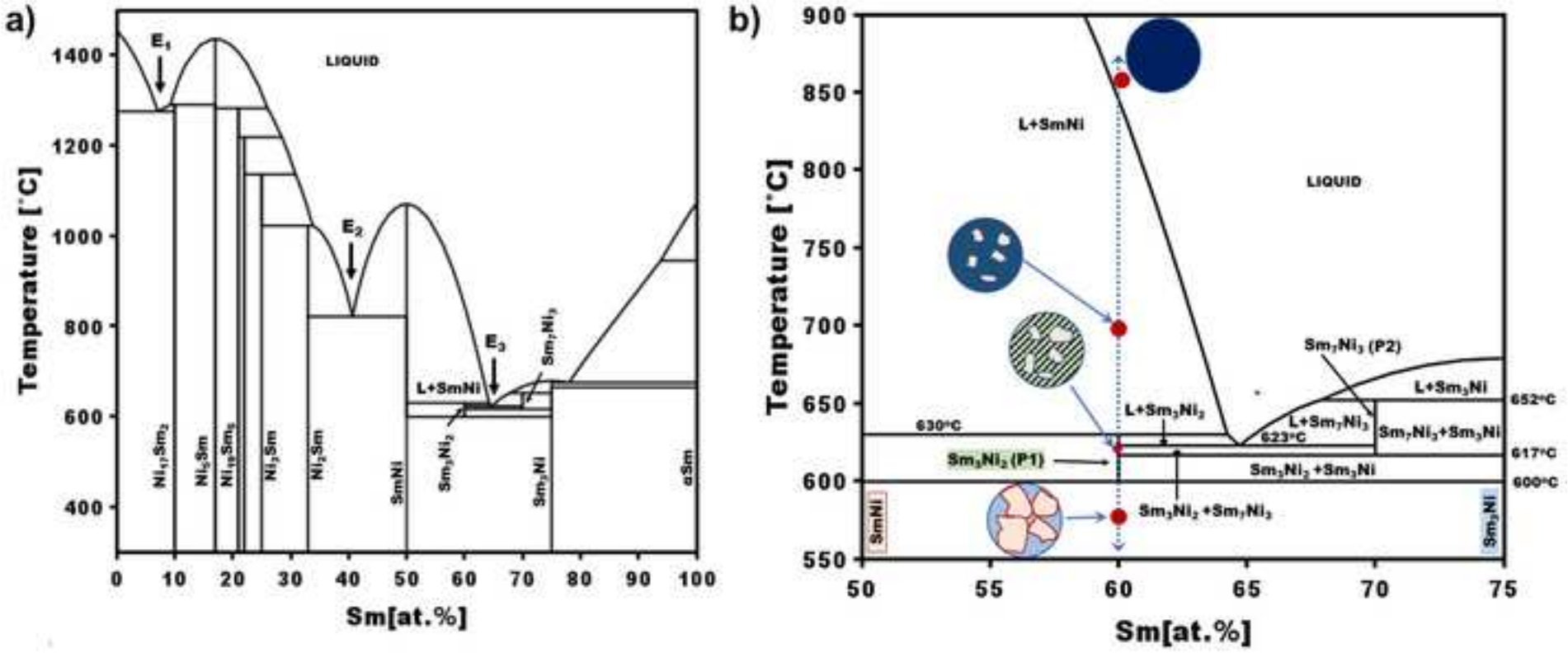

Fig. 1

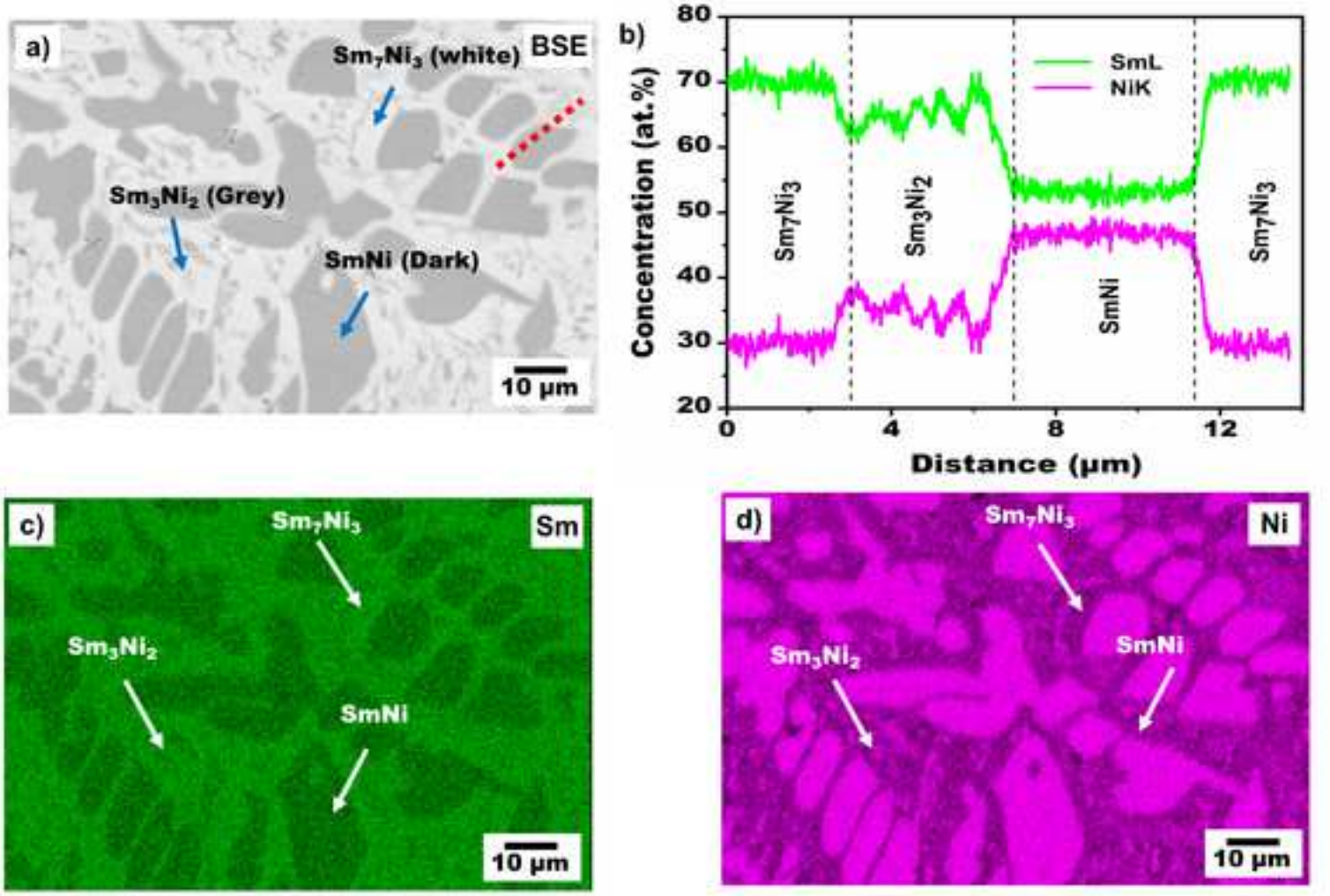

Fig. 2

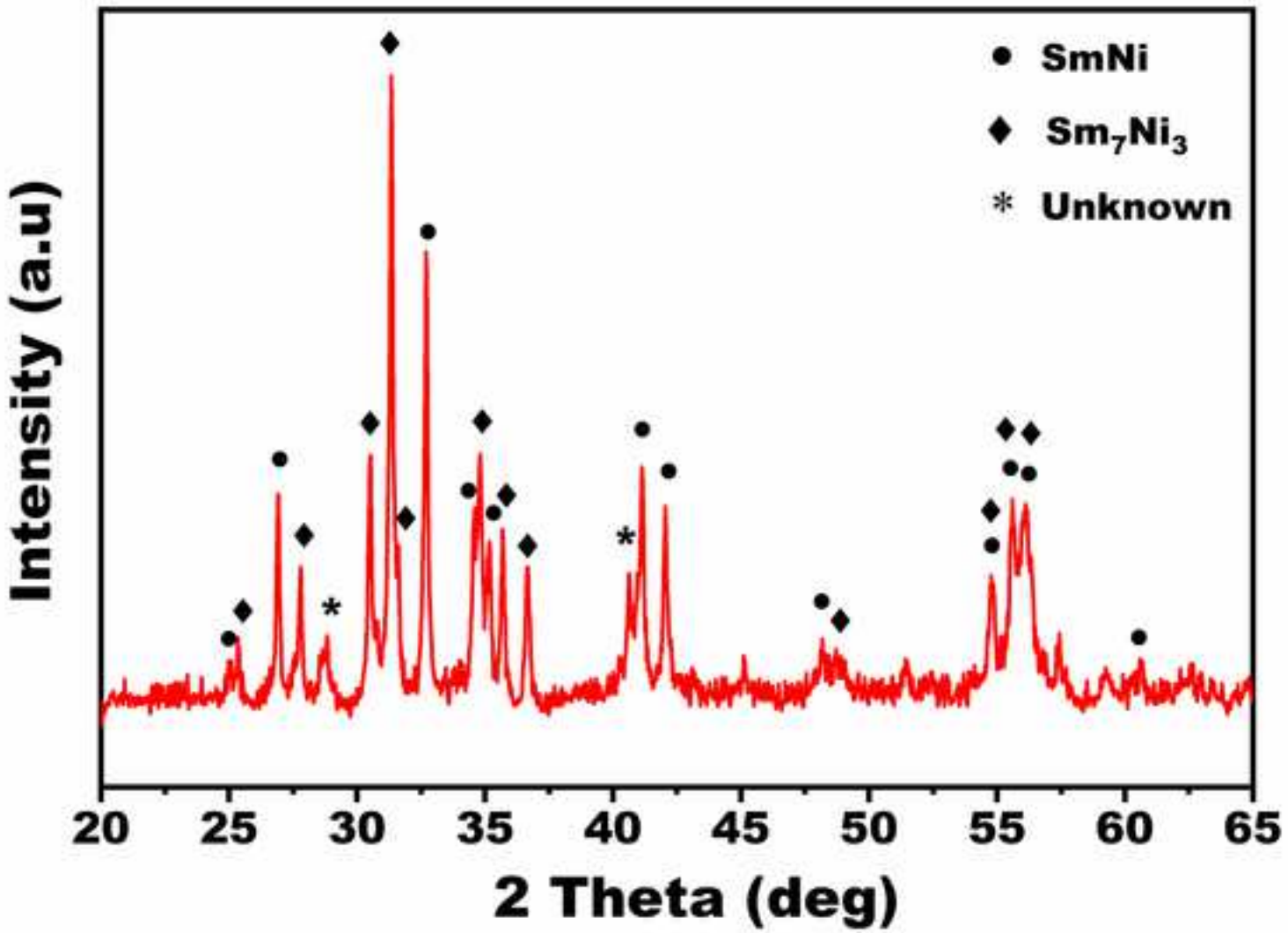

Fig. 3

Figure 4

Click here to access/download;Figure;fig. 4.tif

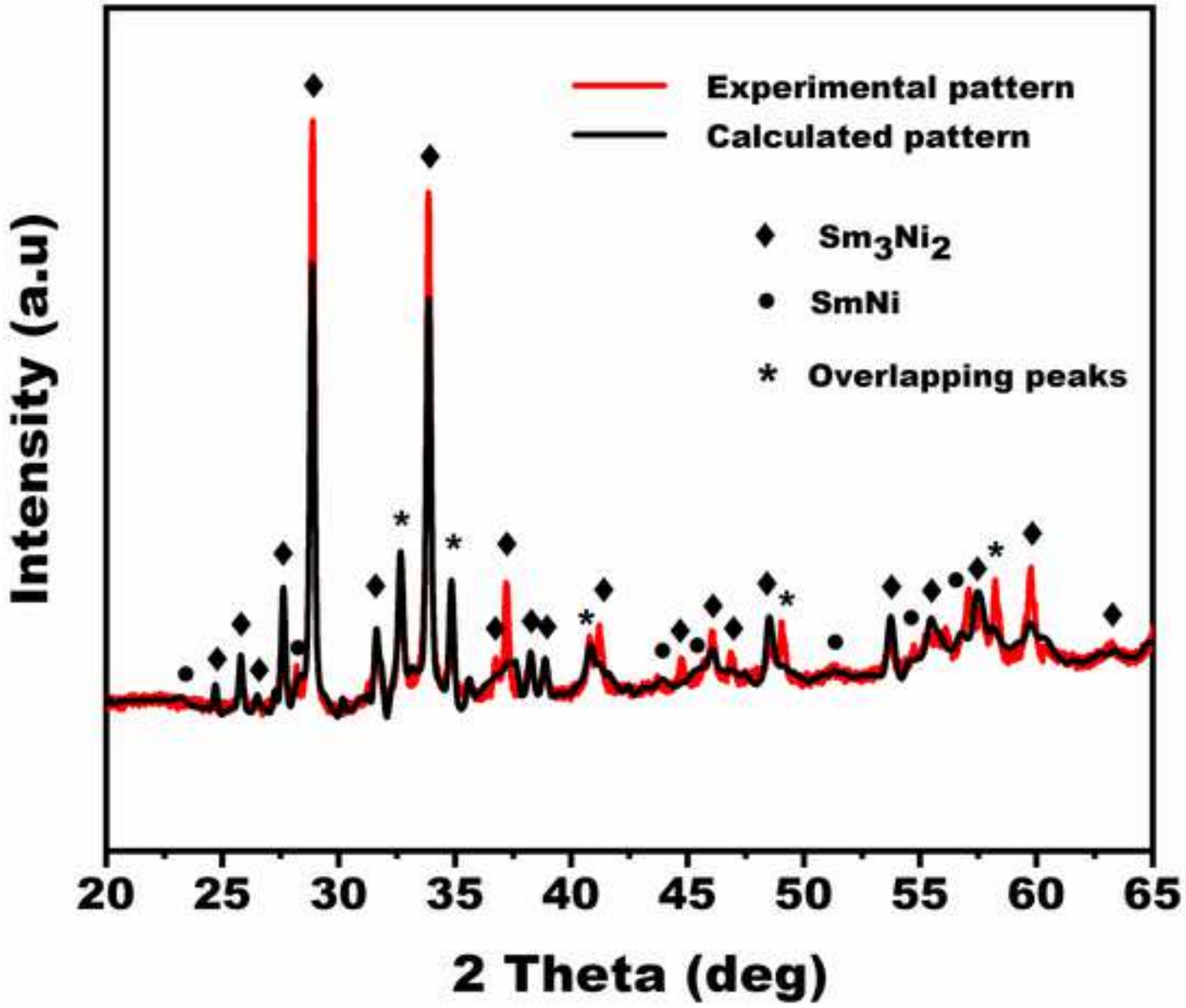

Fig. 4

Figure 5

Click here to access/download;Figure;fig. 5.tif

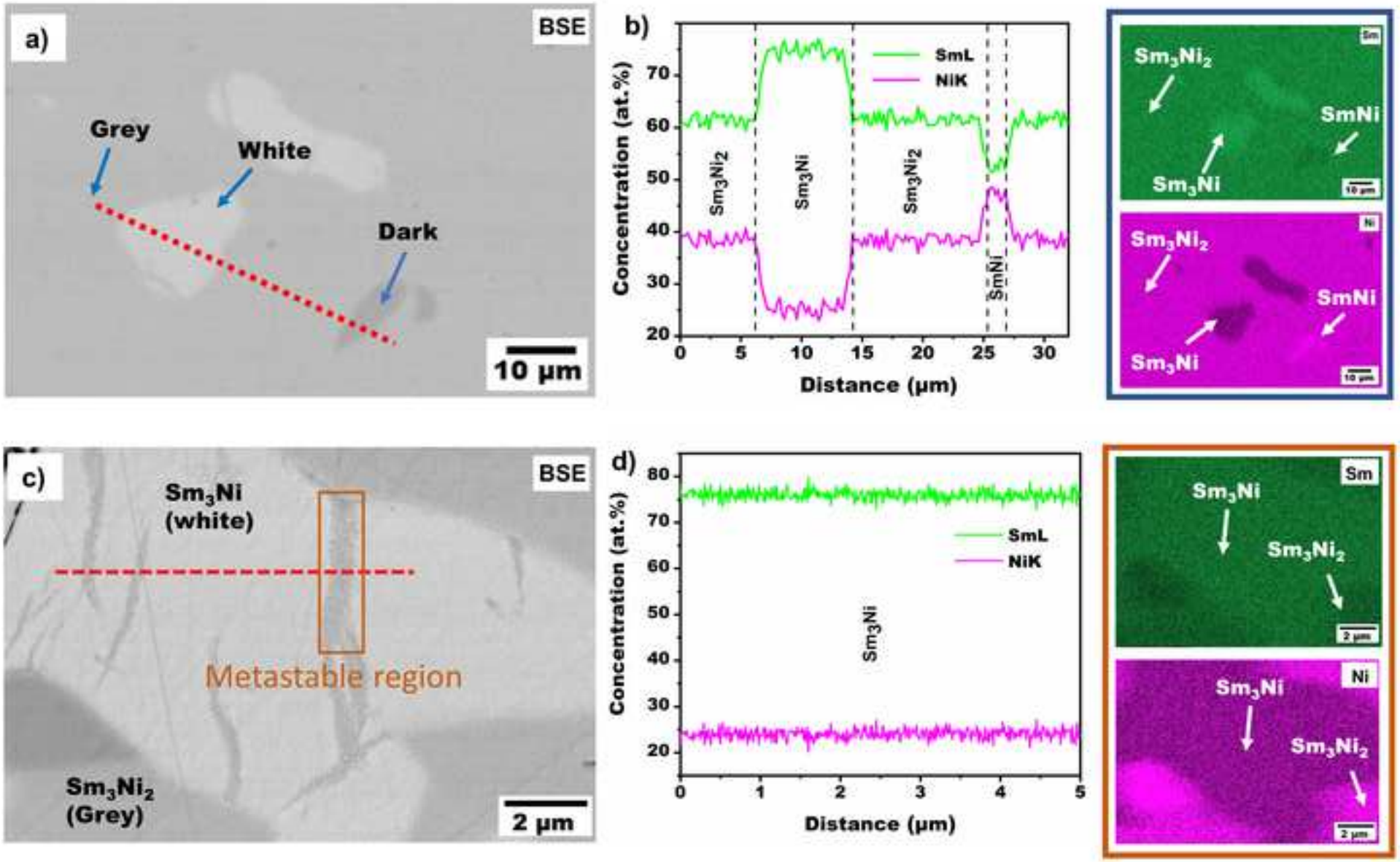

Fig. 5

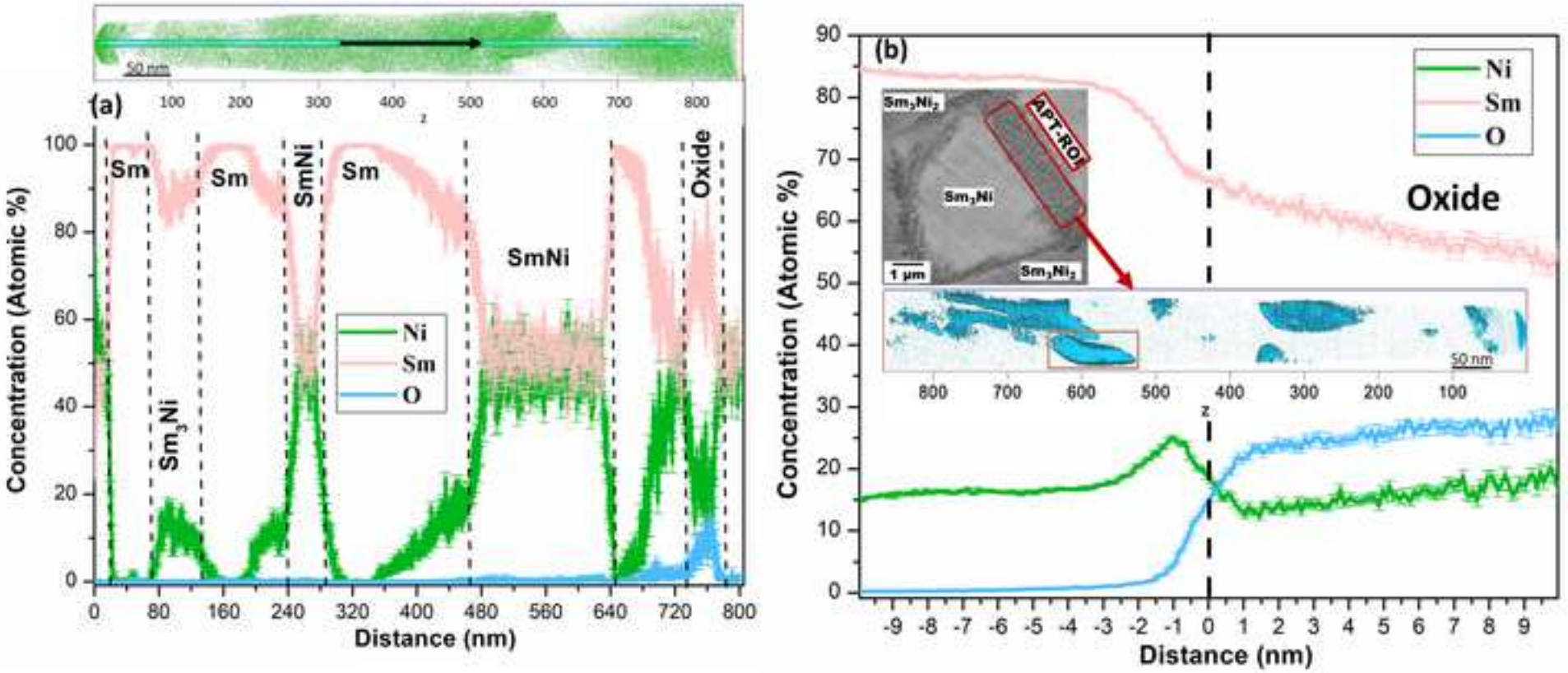

Fig. 6

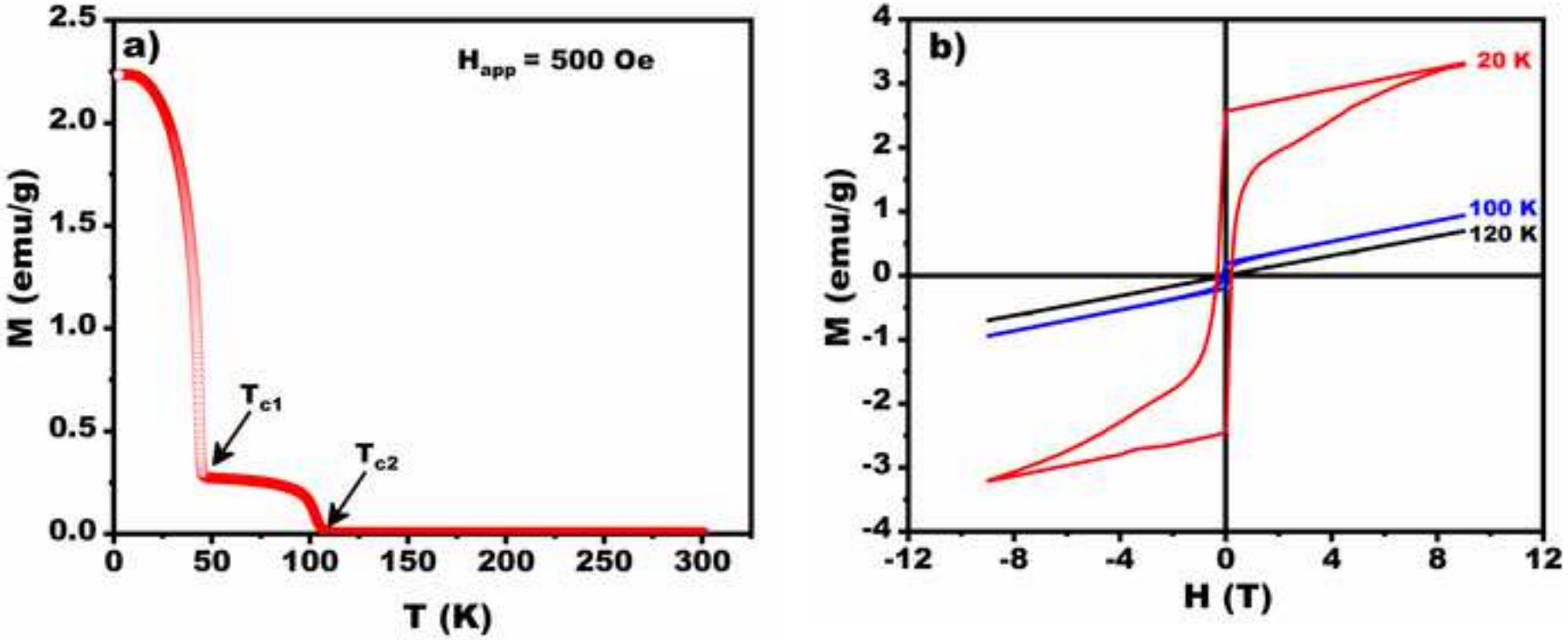

Fig. 7

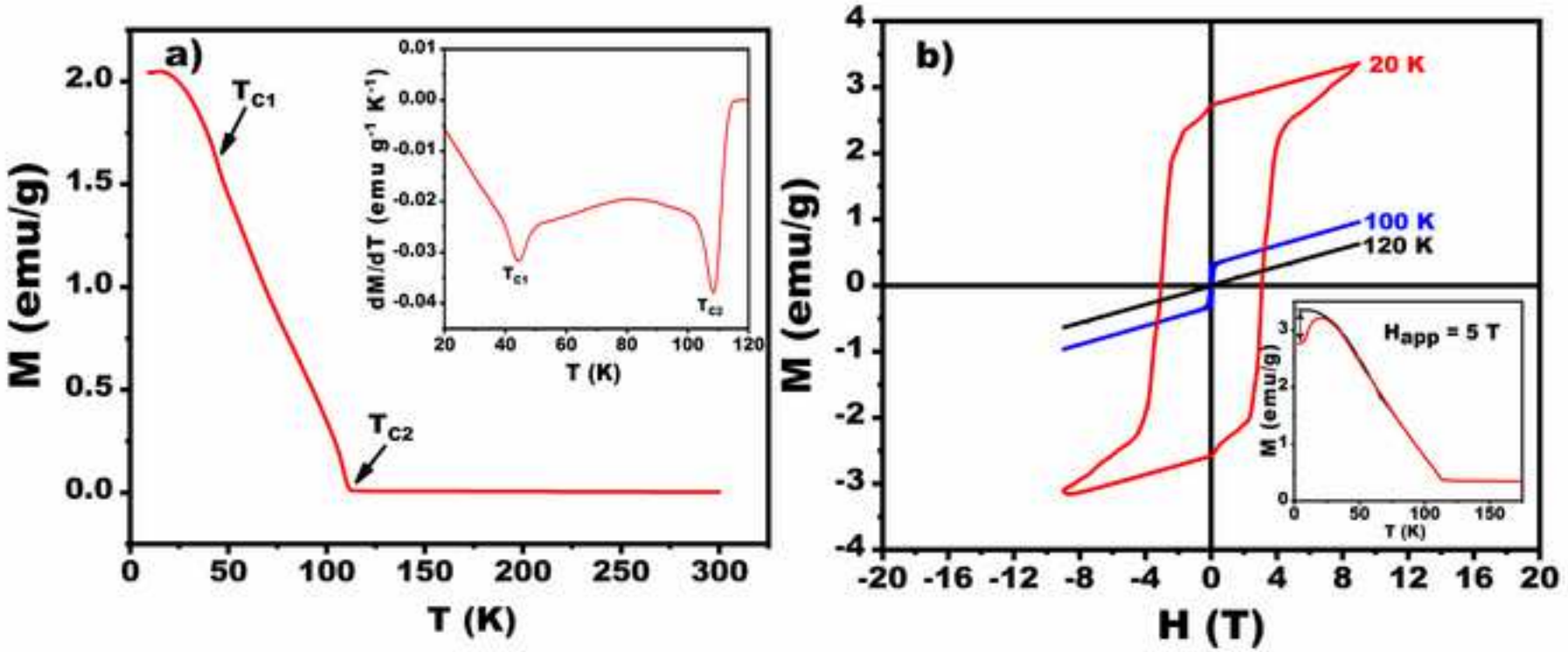

Fig. 8

Declaration of interests

☒The authors declare that they have no known competing financial interests or personal relationships that could have appeared to influence the work reported in this paper.

☐The authors declare the following financial interests/personal relationships which may be considered as potential competing interests: